The Impact of LO Phase Noise in N-Path Filters

Thomas Tapen, Zachariah Boynton, Hazal Yüksel, *Student Member, IEEE*,
Alyssa Apsel, *Senior Member, IEEE*, and Alyosha Molnar

***Abstract*— As passive mixers (N-path filters) are being used more frequently and in more applications, it becomes increasingly important to understand how various non-idealities affect the performance of passive mixer circuits. One such non-ideality is perturbations in the local oscillator (LO), including phase noise. Here, we consider a basic N-path filter and develop a preliminary model to analyze the effects of LO phase perturbations in shunting N-path filters. We do so by developing a transfer function from phase perturbations in the LO to voltage perturbations on a strong RF signal at the mixer's RF port. We find that LO phase noise is suppressed where it is strongest (i.e., for small offset frequencies). As a result the RF spectrum's noise peak does not appear around the signal tone, but rather around the LO frequency, due to the bandpass characteristic generated by a typical capacitive baseband load. These analytical results are verified using numerical and schematic simulation in custom software and Cadence, and they are further confirmed by measurement of a frequency-scaled, board-level implementation of an N-path filter.**

***Index Terms*— Passive mixer, N-path filter, bandpass filtering, SAW-less, phase noise, inductorless filter.**

I. Introduction

PASSIVE-MIXER based (N-path) filters, while known for decades [1], have seen a recent explosion of interest in the field of RF integrated circuits, both as down-conversion mixers [2] and as explicit, tunable RF filters [3]. Perhaps their most striking property stems from their ability to bidirectionally translate impedance across frequency. Specifically, an N-path passive mixer will translate (upconvert) the impedance seen on its N-terminal baseband port to its RF port, and vice-versa. When that baseband impedance is a simple RC low-pass impedance, the result is a band-pass RF impedance with a half-bandwidth equal to the baseband LPF bandwidth, and a center frequency set by the local oscillator (LO) of the mixer. Critically, since center frequency and bandwidth are decoupled, this permits a widely tunable and arbitrarily high Q to be synthesized with baseband circuitry, while simultaneously supporting (through LO generation circuitry) a highly tunable center frequency. This combination of properties is extraordinarily difficult to create using only static (LTI) components. Due to these properties, structures similar to N-path filters have found their way into other interesting application spaces, such as passive mixer-first receiver architectures [4]–[6], full-duplex radio [7], [8], and others [9], [10].

Manuscript received May 21, 2017; revised August 16, 2017 and September 23, 2017; accepted September 24, 2017. Date of publication October 20, 2017; date of current version April 2, 2018. This work supported in part by the National Science Foundation under Grant ECCS-1247915 and Grant EFMA-1641100, in part by the the DARPA CLASS Program, and in part by Google Inc. This paper was recommended by Associate Editor G. Jovanovic Dolecek. *(Corresponding author: Thomas Tapen.)*

The authors are with the Department of Electrical and Computer Engineering, Cornell University, Ithaca, NY 14853 USA (e-mail: tpt26@cornell.edu).

Color versions of one or more of the figures in this paper are available online at http://ieeexplore.ieee.org.

Digital Object Identifier 10.1109/TCSI.2017.2761260

While passive LTI RF filters struggle to offer tunability and high-Q in a small area, they add very little noise to the signal path. If N-path filters are used to replace bulky passive filters, they may not be able to match the noise performance of passives. However, work to date has had little to say about how LO phase noise and other LO perturbations impact N-path filters and other passive mixer applications. When used strictly as down-converters, LO phase noise interacts with input signals in passive mixers exactly as it does in more standard, active mixers: Strong RF signals interact with an LO's phase noise skirt to generate baseband noise around the down-converted RF signal, as shown in Figure 1. Phase noise contributed by the input signal (V_s in Figure 1) has been addressed in [15], and other LO non-idealities like overlap between the N LO pulses have also been analyzed in [6], [14], [15]. It remains unknown how phase noise present on the LO is transferred to the RF port due to RF signals—a critical circuit characteristic for N-path filter applications that are sensitive to noise, such as [4]–[8].

In this paper we introduce for the first time to our knowledge the impact of LO phase perturbations on shunting band-pass N-path filters at an intuitive level, an analytical level, with numerical simulation, and with real-world measurements. In all cases we show that phase perturbations (i.e. phase noise) in the LO does indeed corrupt the RF spectrum when strong RF signals are present, and we also show that the shape of the transfer function, and therefore the output noise spectrum is a strong function of not just the phase noise itself, but of the frequency of RF signals, and the filtering properties of the baseband circuit. The paper is organized as follows: Section II contains initial qualitative analysis of an N-path filter to examine what the expected effects of LO phase noise are on the RF spectrum of an N-path filter. In Section III we quantitatively derive the N-path filter's RF spectrum in the presence of LO phase perturbations. Finally, in Section IV, the results of Section III are compared with various numerical simulations and measurements of a frequency-scaled implementation of an N-path filter to check their validity.

II. Qualitative Look at the RF Noise Spectrum

A schematic of an N-path filter is shown in Figure 3, where V_s is the RF input to the circuit, S_{LO} is the noisy LO, and M_1 is an N-phase passive mixer (where N = 4). To reason

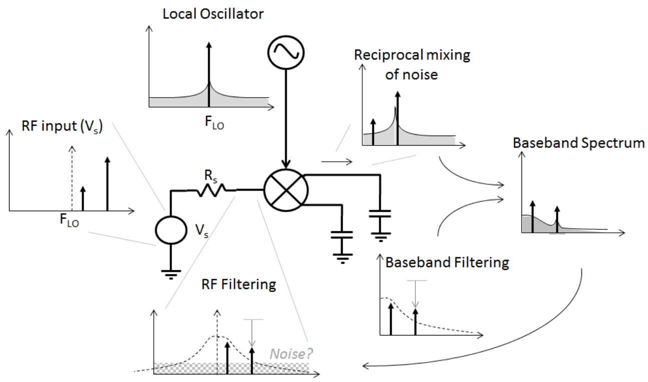

Fig. 1. An example N-path filter with a noisy LO. If the voltage at the RF port is noiseless, standard reciprocal mixing combined with the baseband impedance creates the baseband noise spectrum shown above. However, in an N-path filter, that baseband noise is re-upconverted by the noisy LO, putting noise onto the RF port. A model for the re-upconversion of baseband noise, and the further effects once that noise appears at the RF port are the topics of this paper.

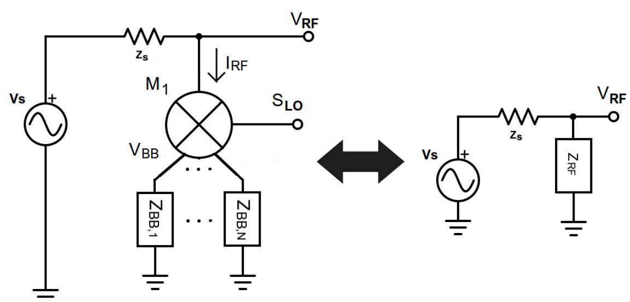

Fig. 2. Comparison of a typical N-path filter with a simple passive filter. N-path filters can synthesize a high-Q bandpass transfer function using baseband circuitry rather than high-Q RF components, as would typically be needed to generate Z_{RF} in a simple passive filter.

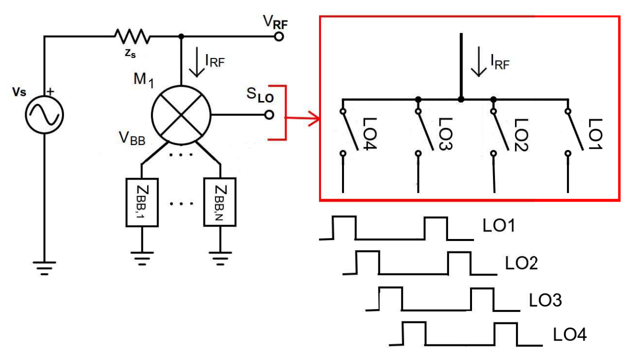

Fig. 3. The circuit under analysis in this paper—an N-path filter built using a passive mixer. In this paper we model the mixer as an ideal, bidirectional multiplier, as shown in the left schematic. However, a more realistic representation of the mixer is shown on the right, where an ideal 4-phase mixer is displayed.

about how phase noise maps from the LO to the RF port, we will treat all aspects of the circuit except the LO as noiseless. We will also ignore all LO harmonic down- and up-conversion effects. As drawn in Figure 3, V_{RF} depends on the source V_s, as well as the upconverted baseband voltage.

A. Noiseless Time Domain Behavior of N-Path Filters

To model the effects of mixing and impedance, we can explicitly separate signal down-conversion (in current mode),

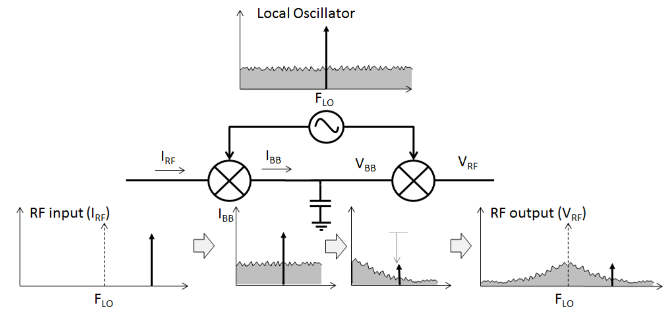

Fig. 4. A qualitative, frequency domain look at the behavior of the circuit in Figure 3 if F_{RF} is far from F_{LO}. Here the white phase noise on the LO is mapped onto the baseband current through the downconversion step, the signal and noise are filtered, and the resulting voltage is upconverted. The upconversion step does not add significant noise close to F_{LO} due to the attenuation of the (out-of-band) signal by the baseband filtering.

the conversion of baseband current to voltage via the baseband impedance, and then the resulting re-upconversion in voltage mode, producing an I-to-V relationship. However, it is important to recognize that these two operations happen simultaneously in the same single set of switches. This separation results in the diagram in Figure 5. Following from left to right, an input current I_{RF} at frequency F_{RF} is multiplied by N windows corresponding to the N non-overlapping LO pulses (N = 8 in this example). The baseband impedance then low-pass filters these current pulses, resulting in N baseband voltages. For an in-band tone (as considered in Figure 5), the current pulses are nearly identical from period to period, as $F_{RF} \approx F_{LO}$. So, for some baseband nodes, current consistently charges the baseband capacitor, maintaining a significant DC level. For an out-of-band input, a single baseband node will end up sampling many different points on the input sinusoid (as F_{RF} and F_{LO} differ significantly), and because the average of a sinusoidal input is 0, no baseband voltages are generated for an out-of-band input. For either case, each of the resulting N baseband voltages are connected to the RF node in sequence. This process generates a staircase representation of the input current as an output voltage V_{RF}, whose amplitude decreases as F_{RF} diverges from F_{LO}.

This process as demonstrated in Figure 5 assumes a number of idealities, one of which is perfect LO pulses. Assumed in our discussion so far are instantaneous rise and fall times, no overlapping between pulses, and no phase noise. While analysis has been done on the effects of non-zero rise and fall times, as well as the effects of overlapping LO pulses [6], [14], [15], it remains unknown how LO phase noise affects the operation of an N-path filter. To begin our analysis, we first consider the noise-shaping effects of the baseband impedance for an out-of-band input. Then we look from a time-domain perspective and find that we should expect close-in phase noise to be suppressed by the circuit for all input frequencies.

B. Qualitative Noise Analysis of N-Path Filters

For an out-of-band RF signal (Figure 4), cyclic sampling onto the baseband capacitances will convert the RF signal to baseband signal current as well as noise current resulting from

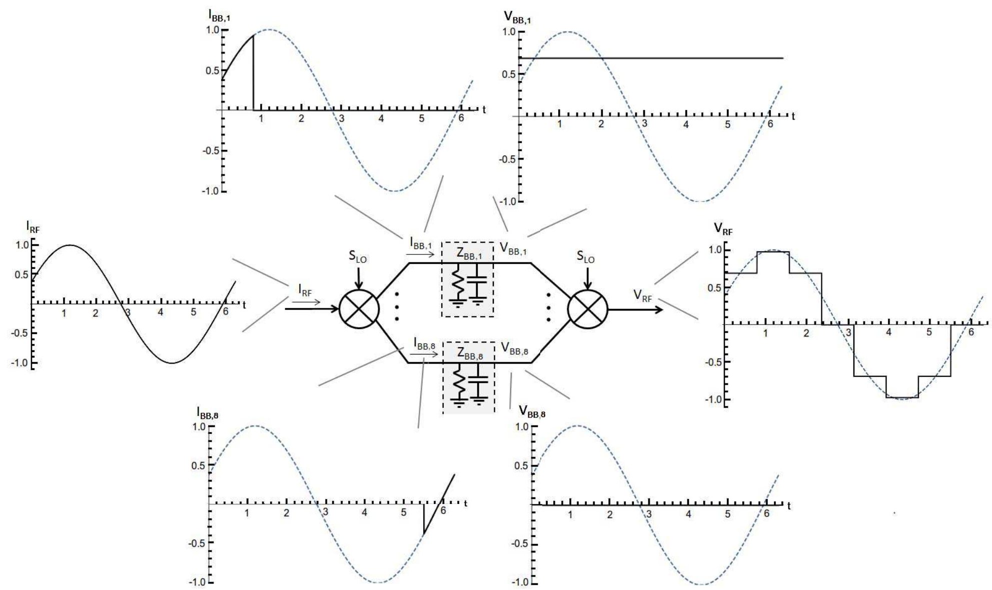

Fig. 5. An illustration of how cyclic down- and up-sampling occurs in an N-path filter with ideal, noiseless LO pulses. Here we assume a in-band current input I_{RF} and chose N = 8. First the input current is windowed by the LO pulses across N baseband nodes, then the capacitive baseband impedance averages the baseband current and generates a baseband voltage. Finally, the N baseband voltages are recombined by the same LO generating a re-upconverted voltage.

the RF signal interacting with LO phase noise. The baseband impedance then converts these currents to a voltage while low-pass filtering both. This results in significant suppression of the (out-of-band) signal and shapes the noise. The resulting baseband signal is then re-upconverted, through cyclic upsampling from the baseband capacitors. Baseband noise on the sampling capacitors is directly upconverted and appears at the RF port as a noise peak around F_{LO}. However, additional noise is added during upconversion just as it was for downconversion. This noise arises from the RF signal interacting with LO phase noise, and because the RF signal was greatly attenuated by the baseband impedance, we can assume for a far enough out-of-band input, the upconversion noise power is small compared with that at the peak around F_{LO}.

For an in-band tone, we cannot simply ignore the noise from upconversion, as the signal is not attenuated by the baseband impedance. If the noise terms introduced by up- and down-conversion are independent, the results simply sum—however, we expect the noise will *not* be independent, as the same LO produces both up- and downconversion simultaneously.

If we return to time-domain analysis as in Figure 5, we can consider what happens if each LO pulse's edges vary with some noise from cycle to cycle in time. Rapid variations in edge timing (far-out phase noise) introduce errors in each of the baseband currents that change on a near per-cycle basis. These rapidly changing error currents are filtered out by the baseband capacitors, but are then re-introduced by the upconversion step. So, given an in-band tone, the effects for far-out phase noise are the reverse of the out-of-band case discussed above—The baseband filtering makes the noise from downconversion negligible, and the noise introduced during upconversion dominates.

For slowly varying edge timing (close-in phase noise), the story is different. Errors introduced during downconversion in this case are slowly varying, and therefore are not filtered by the baseband impedance. Because re-upconversion happens simultaneously in the same N switches as downconversion, the exact same timing errors are repeated during upconversion. So, although there exists slowly varying noise in the baseband, having the identical timing errors in re-upconversion means the baseband voltage will still map out the input signal accurately. Therefore, almost no noise power is contributed by close-in phase noise. The resulting RF noise spectrum for an in-band tone is shown in Figure 6—far from F_s and F_{LO} the upconversion noise which was not filtered by the baseband dominates, however close-in noise is, in effect, canceled and a notch appears in the RF spectrum. As will be seen in the next section, close-in noise is in fact canceled at all times, not just for an in-band tone.

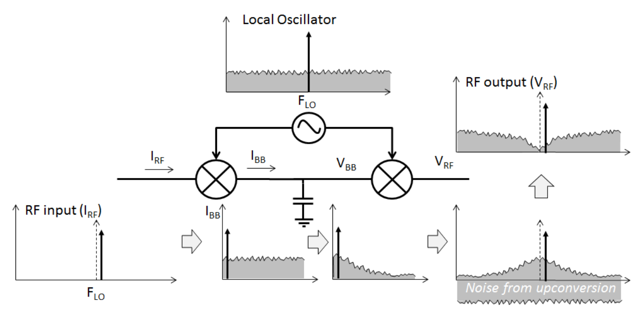

Fig. 6. A qualitative, frequency domain analysis of an N-path filter with LO phase noise given an in-band RF input current. As discussed in the text, close-in noise is canceled, and far-out phase noise from the upconversion step dominates over that of the downconversion step due to the baseband filtering characteristic.

III. Mathematical Analysis of N-path Filters

Existing quantitative analysis of passive mixers can be done by modeling the impedance looking into the RF port over frequency with an LTI model [11], [12]. While this is convenient, passive mixers cannot be modeled with an

TABLE I

TABLE OF MATHEMATICAL TERMS USED IN THIS DERIVATION

Name			Definition
N			Number of switches used in the N-path filter.
V_s			RF input signal, a sinusoid with amplitude A at ω_s.
Z_s			RF source impedance.
$Z_{BB,i}$			Impedance loading baseband port i of the passive mixer. $i \in [1, N]$.
$Z_{BB,I}$			The effective impedance loading the I component of the baseband signal.
$Z_{BB,Q}$			The effective impedance loading the Q component of the baseband signal.
Z_{BB}			Impedance presented across all N baseband ports. $Z_{BB} = Z_{BB,1}\|\|Z_{BB,2}\|\|...\|\|Z_{BB,N}$ for an N-path filter. $Z_{BB} = Z_{BB,I}\|\|Z_{BB,Q}$ for I/Q analysis as performed below (see Figure 7).
—	Z_{high}		$Z_{BB}(\omega)$ evaluated at $(\omega + \omega_{LO})$
—	Z_{low}		$Z_{BB}(\omega)$ evaluated at $(\omega - \omega_{LO})$
V_{RF}			Voltage at the RF port of the mixer in Figure 3.
—	$V_{RF,s}$		Signal component of V_{RF}. This term has frequency ω_s.
—	$V_{RF,n}$		Component of V_{RF} generated due to phase perturbations in S_{LO}. This term has frequency $\omega_s \pm \omega_n$.
I_{RF}			Current into the RF port of the mixer in Figure 3.
—	$I_{RF,s}$		Signal component of I_{RF}. This term has frequency ω_s.
—	$I_{RF,n}$		Component of I_{RF} generated due to phase perturbations in S_{LO}. This term has frequency $\omega_s \pm \omega_n$.
S_{LO}			Quadrature LO signal, including phase perturbations.
—	$S_{LO,I}$		I component of the quadrature LO signal.
—	—	$S_{LO,Is}$	Signal component of $S_{LO,I}$. This term has frequency ω_{LO}.
—	—	$S_{LO,In}$	Phase perturbation component of $S_{LO,I}$. This term has frequency $\omega_{LO} \pm \omega_n$.
—	$S_{LO,Q}$		Q component of the quadrature LO signal.
—	—	$S_{LO,Qs}$	Signal component of $S_{LO,Q}$. This term has frequency ω_{LO}.
—	—	$S_{LO,Qn}$	Phase perturbation component of $S_{LO,Q}$. This term has frequency $\omega_{LO} \pm \omega_n$.
$I_{BB,I}$			I component of the baseband current.
—	$I_{BB,Is}$		Signal component of $I_{BB,I}$.
—	—	$I_{BB,Is,low}$	Component of $I_{BB,Is}$ generated by downconversion of $I_{RF,s}$. This term has frequency $\omega_s - \omega_{LO}$.
—	—	$I_{BB,Is,high}$	Component of $I_{BB,Is}$ generated by upconversion of $I_{RF,s}$. This term has frequency $\omega_s + \omega_{LO}$.
—	$I_{BB,In}$		Component of $I_{BB,I}$ caused by phase perturbations in $S_{LO,I}$.
—	—	$I_{BB,In,low}$	Component of $I_{BB,In}$ generated by noisy downconversion of $I_{RF,s}$. This term has frequency $\omega_s - \omega_{LO} \pm \omega_n$.
—	—	$I_{BB,In,high}$	Component of $I_{BB,In}$ generated by noisy upconversion of $I_{RF,s}$. This term has frequency $\omega_s + \omega_{LO} \pm \omega_n$.
$I_{BB,Q}$			Q component of the baseband current. Just as with the I component of baseband current, $I_{BB,Q}$ can be decomposed into signal and noise components, and then further into up and downconversion products.
Z_{mix}			Effective impedance of the mixer looking into its RF port ignoring any effects of phase noise in S_{LO}.
Z_n			Effective impedance that captures how an input RF current at ω_s is converted to an RF voltage at $\omega_s \pm \omega_n$.

typical LTI impedance when phase noise is present on the LO, as some of the signal power will be shifted to other frequencies by phase perturbations (as we saw qualitatively above). To analyze what happens when phase noise is present, we will proceed as follows:

First, we will analyze the circuit in Figure 3 assuming a noiseless LO. To do so, we will derive the RF-current-to-RF-voltage characteristic of the passive mixer in isolation by modeling the mixer the same way as in Section II, except we will rigorously keep track of both I and Q mixing paths. Once the I-to-V characteristic is established, that result can be used as part of a feedback loop to find the behavior of the full system, including the source impedance Z_s. Because the LO is noiseless, we will find that the I-to-V characteristic is simply an input frequency-dependent impedance as expected.

We will then replace the noiseless LO with an LO containing phase perturbations (noise), and repeat the analysis. This time, the I-to-V characteristic of the passive mixer will consist of two components: 1) The signal current ($I_{RF,s}$) to signal voltage ($V_{RF,s}$) behavior without phase perturbations, and 2) The signal current ($I_{RF,s}$) to noise voltage ($V_{RF,n}$) behavior that captures how voltage is generated at frequencies other than the frequency of the input current.

Finally, given how an input current signal generates an RF voltage including both signal and noise components, we can solve for the full circuit behavior, and find the resulting V_{RF} including the effects of both Z_s and phase perturbations in the LO interacting with the baseband impedance Z_{BB}.

In our analysis, we define many terms to keep our expressions manageable. Table I serves as a reference for all of the terms defined during the derivation for the convenience of readers.

A. Signal Propagation

As per the roadmap above, we start by assuming a noiseless LO and looking at how a current signal into the mixer ($I_{RF,s}$) at frequency ω_s produces an output voltage ($V_{RF,s}$). We can model the mixer as in Figure 7 with two quadrature multipliers, one in the current domain, and the other in the voltage domain, separated by an impedance which filters the current signals as it transforms them into voltages.

We start by describing the RF current into the mixer as:

$$\begin{aligned} I_{RF,s}(t) &= A\cos(\omega_s t + \theta) \\ I_{RF,s}(\omega) &= \frac{A}{2}\left[e^{-j\theta}\delta(\omega - \omega_s) + e^{j\theta}\delta(\omega + \omega_s)\right] \end{aligned} \tag{1}$$

and describing the (for now noiseless) quadrature LO:

$$\begin{aligned} S_{LO,Is}(t) &= \cos(\omega_{LO} t) \\ S_{LO,Qs}(t) &= -\sin(\omega_{LO} t) \end{aligned} \tag{2}$$

$$\begin{aligned} S_{LO,Is}(\omega) &= \frac{1}{2}\left[\delta(\omega - \omega_{LO}) + \delta(\omega + \omega_{LO})\right] \\ S_{LO,Qs}(\omega) &= \frac{j}{2}\left[\delta(\omega - \omega_{LO}) - \delta(\omega + \omega_{LO})\right] \end{aligned} \tag{3}$$

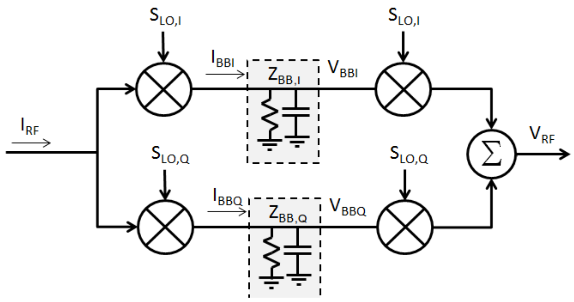

Fig. 7. The current-to-voltage behavior of the passive mixer in Figure 3, with down and upconversion separated into explicit steps. First, the RF input current is multiplied by the quadrature LO, then the baseband impedance converts that current to a voltage, and finally the result is re-upconverted in the voltage domain to produce a voltage at the mixer's RF port.

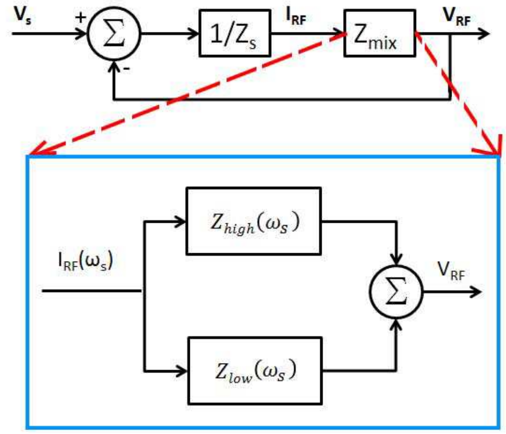

Fig. 8. An LTI block diagram describing the circuit in Figure 3 assuming an ideal, noiseless LO. The mixer can be represented with an impedance Z_{mix}, which is the sum of the baseband impedance evaluated at $\omega + \omega_{LO}$ and $\omega - \omega_{LO}$ (see Table I).

Given these definitions, we can solve for $V_{RF,s}$ by convolving $I_{RF,s}$ with $S_{LO,Is}$ and $S_{LO,Qs}$ to generate I and Q output currents at $\omega = \omega_s \pm \omega_{LO}$. Then we can multiply these currents by $Z_{BB,I}(\omega)$ and $Z_{BB,Q}(\omega)$ to generate I and Q voltages, and finally convolving once more with $S_{LO,Is}$ and $S_{LO,Qs}$ respectively. This gives the result:

$$\begin{aligned} V_{RF,s} = &\Big[Z_{BB,I}(\omega)[I_{RF,s}(\omega) * S_{LO,Is}(\omega)]\Big] * S_{LO,Is}(\omega) \\ &+ \Big[Z_{BB,Q}(\omega)[I_{RF,s}(\omega) * S_{LO,Qs}(\omega)]\Big] * S_{LO,Qs}(\omega) \end{aligned} \tag{4}$$

which simplifies to:

$$\begin{aligned} V_{RF,s} &= I_{RF,s}\Big[Z_{BB}(\omega_s - \omega_{LO}) + Z_{BB}(\omega_s + \omega_{LO})\Big] \\ &= I_{RF,s} Z_{mix}(\omega_s) \end{aligned} \tag{5}$$

given:

$$\begin{aligned} Z_{BB}(\omega) &= Z_{BB,I}(\omega)||Z_{BB,Q}(\omega) \\ Z_{mix}(\omega_s) &\equiv Z_{BB}(\omega_s - \omega_{LO}) + Z_{BB}(\omega_s + \omega_{LO}) \end{aligned} \tag{6}$$

While the individual nested convolution operations in equation (5) lead to terms at frequencies $\omega_s - 2\omega_{LO}$, ω_s, and $\omega_s + 2\omega_{LO}$, summing I and Q paths cancels all but the ω_s terms regardless of the baseband filtering in a similar way to standard image rejection. This returns the signal to its original input frequency, and allowing us to define an LTI impedance Z_{mix} as previously asserted. The critical implication of this result is that the RF voltage's amplitude and phase depend on the âŁœbasebandâŁž impedance at both the sum and difference frequencies, summed together. For a typical RC low-pass Z_{BB}, this results in band-pass behavior in $Z_{mix}(\omega)$ with peaks at $\omega = \pm\omega_{LO}$.

Finally, to incorporate Z_s, we describe the full circuit in Figure 3 using the block diagram in Figure 8, which allows us to find the transfer function from V_s to V_{RF} of the full circuit (without LO phase noise):

$$\frac{V_{RF,s}(\omega_s)}{V_s(\omega_s)} = \frac{Z_{mix}(\omega_s)}{Z_{mix}(\omega_s) + Z_s(\omega_s)} \tag{7}$$

B. Phase Perturbation Model

Now that we have a description of how signal propagates through the system, we can look at how LO phase perturbations can interact with the signal to generate perturbation terms at frequencies other than ω_s in V_{RF}. $S_{LO,I}$ and $S_{LO,Q}$ will describe a quadrature LO with a small amount of phase noise. Starting with a cosine containing a random noise function $\psi(t)$ to model phase perturbations, we assume that all the frequency components of $\psi(t)$'s Fourier Series are all small ($\epsilon_n << 1$, with random phase ϕ_n).

$$\begin{aligned} S_{LO,I}(t) &= \cos[\omega_{LO}t + \psi(t)] \\ &= \cos\left[\omega_{LO}t + \sum_{n=0}^{\infty} 2\epsilon_n \cos(\omega_n t + \phi_n)\right] \end{aligned} \tag{8}$$

Since our primary interest is in how phase perturbations of the LO translate to voltage perturbations on the RF port, we can analyze how a perturbation at a given frequency offset (ω_n) translates to a given perturbation in V_{RF}. Put another way, we are interested in an offset frequency-dependent transfer function from LO phase perturbations to RF voltage.

We pick out a given term of the Fourier Series of $\psi(t)$ to analyze in depth. In order to capture how all frequencies of phase noise reach the final output, the frequency of this term (ω_n) will be swept from 0 to ∞ and the results superposed. We apply the assumption that ϵ_n is small in equation (9) by using a first-order Taylor expansion on $\cos(x)$.

$$\begin{aligned} S_{LO,I}(t) &= \cos[\omega_{LO}t + 2\epsilon_n \cos(\omega_n t + \phi_n)] \\ &= \cos(\omega_{LO}t) - \epsilon_n \sin[(\omega_{LO} + \omega_n)t + \phi_n] \\ &\quad - \epsilon_n \sin[(\omega_{LO} - \omega_n)t - \phi_n] \\ &= S_{LO,Is} + \epsilon_n S_{LO,In} \end{aligned} \tag{9}$$

Similarly we define $S_{LO,Q}(t) = \sin[\omega_{LO}t + \psi(t)]$, and the same analysis is performed as was just done for $S_{LO,I}$, we find an expression for $S_{LO,Q}(t)$:

$$\begin{aligned} S_{LO,Q}(t) &= \sin(\omega_{LO}t) + \epsilon_n \cos[(\omega_{LO}+\omega_n)t+\phi_n] \\ &\quad + \epsilon_n \cos[(\omega_{LO}-\omega_n)t-\phi_n] \\ &= S_{LO,Qs} + \epsilon_n S_{LO,Qn} \end{aligned} \tag{10}$$

C. Formulation of Interactions Between Signal and Phase Noise

Next we analyze the I_{RF} to V_{RF} interactions as in Section A, simply substituting equation (9) for $S_{LO,Is}$. For compactness, we will derive signal-noise interactions only for the I path. The Q path yields similar results, but shifted by $\pi/2$ radians.

$$\begin{aligned} S_{LO,I}(\omega) &= FT\{S_{LO,Is}(t) + \epsilon_n S_{LO,In}(t)\} \\ &= S_{LO,Is}(\omega) + \epsilon_n S_{LO,In}(\omega) \end{aligned} \tag{11}$$

Since our goal for now is to find how an input current at the signal frequency generates an output voltage at various frequencies, we plug in $I_{RF,s}(t) = A\cos(\omega_s t + \theta)$ exactly as in Section A to find the I (and Q) components of the baseband current:

$$\begin{aligned} I_{BB,I} &= I_{RF,s} * (S_{LO,Is} + \epsilon_n S_{LO,In}) \\ &= I_{BB,Is,low} + \epsilon_n I_{BB,In,low} \\ &\quad + I_{BB,Is,high} + \epsilon_n I_{BB,In,high} \end{aligned} \tag{12}$$

where the frequency of each term is noted in Table I.

With the noisy LO used for current-mode mixing, we have the same baseband signal terms at $\omega_s \pm \omega_{LO}$ ($I_{BB,Is,low}$ and $I_{BB,Is,high}$), but we also have terms resulting from the phase perturbation on the LO: $I_{BB,In,low}$, $I_{BB,In,high}$, $I_{BB,Qn,low}$, and $I_{BB,Qn,high}$. Once again, these signals interact with the baseband impedance, producing $V_{BB,I}$ and $V_{BB,Q}$, however there is one added complication. Because $S_{LO,In}$ and $S_{LO,Qn}$ have components at two separate frequencies, we cannot write a single frequency with which to evaluate Z_{BB} when finding how the current noise terms ($I_{BB,In,low}$, etc.) are converted to voltage noise terms ($V_{BB,In,low}$, etc.). To avoid expanding these noise terms even further, we introduce a shorthand "$\pm\omega_n$", which is used to indicate that there are two frequencies to be evaluated in each noise term.

$$\begin{aligned} V_{BB,In,high} &= \epsilon_n I_{BB,In,high} Z_{BB,I}(\omega_s + \omega_{LO} \pm \omega_n) \\ V_{BB,In,low} &= \epsilon_n I_{BB,In,low} Z_{BB,Q}(\omega_s - \omega_{LO} \pm \omega_n) \end{aligned} \tag{13}$$

$$\begin{aligned} V_{BB,I} &= V_{BB,Is,high} + V_{BB,Is,low} \\ &\quad + V_{BB,In,high} + V_{BB,In,low} \end{aligned} \tag{14}$$

When these voltage signals are then re-upconverted, the result will include four terms: 1) The signal term from section A ($V_{RF,s}$), 2) The baseband noise from the above equation multiplied by the primary LO tone, 3) A new noise term introduced by the phase perturbations in the LO interacting with the baseband signal, 4) The baseband noise translated by

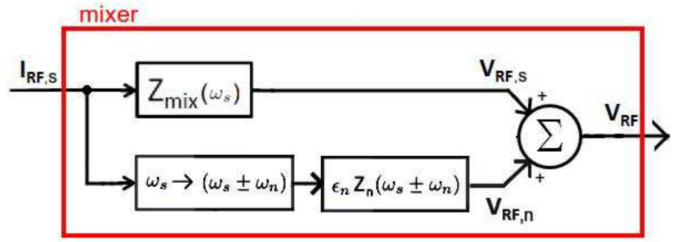

Fig. 9. A model for the mixer including an LO with phase perturbations at the offset frequency $\pm\omega_n$. V_{RF} contains an identical component to the noiseless case ($V_{RF,s}$), and a new term which is translated in frequency and then sees the effective impedance Z_n.

phase perturbations rather than the primary LO tone.

$$\begin{aligned} V_{RF} &= V_{BB,I} * (S_{LO,Is} + \epsilon_n S_{LO,In}) \\ &\quad + V_{BB,Q} * (S_{LO,Qs} + \epsilon_n S_{LO,Qn}) \\ V_{RF} &= V_{RF,s} + \epsilon_n(\text{upconverted BB noise}) \\ &\quad + \epsilon_n(\text{BB signal upconverted by noise}) \\ &\quad + \epsilon_n^2(\text{BB noise upconverted by noise}) \end{aligned} \tag{15}$$

The last term is of magnitude ϵ_n^2 and so can be neglected under the assumption of small ϵ_n. Additionally, the quadrature mixing will eliminate images at $\omega_s + 2\omega_{LO} \pm \omega_n$ and $\omega_s - 2\omega_{LO} \pm \omega_n$ generated by this upconversion step the same as in section A with the signal terms. If V_{RF} is expanded and simplified (see Appendix A), the noise terms appear at only two frequencies $\omega_s \pm \omega_n$:

$$\begin{aligned} V_{RF} &= V_{RF,n} + V_{RF,s} \\ &= \epsilon_n \left[I_{RF,s} * (S_{LO,Is} * S_{LO,In} + S_{LO,Qs} * S_{LO,Qn}) \right] \\ &\quad \cdot \Big[Z_{BB}(\omega_s + \omega_{LO}) - Z_{BB}(\omega_s - \omega_{LO}) \\ &\quad + Z_{BB}(\omega_s - \omega_{LO} \pm \omega_n) \\ &\quad - Z_{BB}(\omega_s + \omega_{LO} \pm \omega_n) \Big] + V_{RF,s} \end{aligned} \tag{16}$$

In equation (16), $V_{RF,s}$ represents the result from section A ($I_{RF,s}Z_{mix}$), while the remaining term $V_{RF,n}$ represents the new effects caused by phase perturbations in the LO. After simplifying as in Appendix A, we find that $V_{RF,n}$ can be written as the signal current $I_{RF,s}$ (shifted in frequency by the various LO components to $\omega_s \pm \omega_n$) multiplied by a new apparent impedance, which depends in part on ω_n (Figure 9). In this form, $[Z_{BB}(\omega_s + \omega_{LO}) - Z_{BB}(\omega_s - \omega_{LO})]$ constitutes the component of $V_{RF,n}$ caused by upconversion of baseband signal by phase perturbations, while $[Z_{BB}(\omega_s - \omega_{LO} \pm \omega_n) - Z_{BB}(\omega_s + \omega_{LO} \pm \omega_n)]$ corresponds to baseband noise generated during down-conversion being upconverted by the main LO signal. We can combine all of these impedance terms into a single noise "impedance" Z_n below:

$$\begin{aligned} Z_n(\omega) \equiv \Big[& Z_{BB}(\omega_s + \omega_{LO}) - Z_{BB}(\omega_s - \omega_{LO}) \\ & + Z_{BB}(\omega - \omega_{LO}) - Z_{BB}(\omega + \omega_{LO}) \Big] \end{aligned} \tag{17}$$

D. Noise Interactions With Z_s

To summarize our progress so far, we take a moment to collect the results of previous sections. They are summarized

TABLE II
SUMMARY OF ANALYTICAL RESULTS FROM PREVIOUS SECTIONS

Equation	Description
$V_{RF,s} = I_{RF,s} Z_{mix}(\omega_s)$	The RF voltage generated due to a current input $I_{RF,s}$ given a noiseless, ideal LO.
$\frac{V_{RF,s}(\omega_s)}{V_s(\omega_s)} = \frac{Z_{mix}(\omega_s)}{Z_{mix}(\omega_s)+Z_s(\omega_s)}$	The RF voltage present given an input signal V_s connected through a source impedance Z_s assuming an ideal LO.
$V_{RF,n} = \epsilon_n Z_n(\omega_s \pm \omega_n)\left[I_{RF,s} * (S_{LO,Is} * S_{LO,In} + S_{LO,Qs} * S_{LO,Qn})\right]$	The RF voltage generated by phase perturbations in the LO.

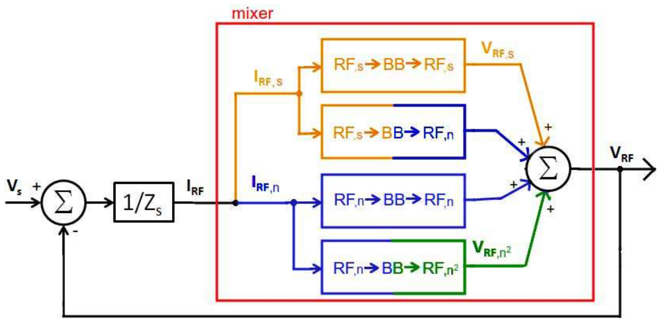

Fig. 10. Modifying Figure 8 with our noisy mixer model from Figure 9 gives this block diagram. Each color represents voltage/current at a specific frequency: orange is at ω_s, blue is at $\omega_s \pm \omega_n$, and green is at $\omega_s \pm 2\omega_n$. Because the V_{RF,n^2} term is of order ϵ_n^2, we ignore its contribution to V_{RF}. Therefore, I_{RF} only contains significant components at ω_s and $\omega_s \pm \omega_n$ ($I_{RF,s}$ and $I_{RF,n}$, respectively).

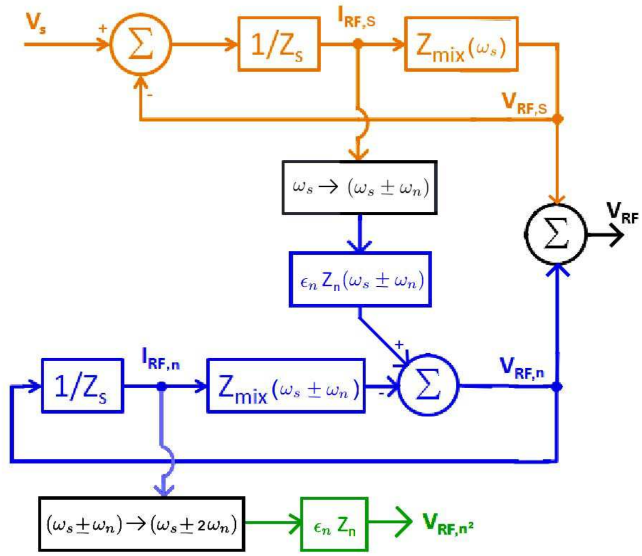

Fig. 11. The result if components of Figure 10 are re-arranged according to frequency so that LTI analysis can be used to resolve the feedback loop present in the system. The same color scheme from Figure 10 applies.

in Table II above. To complete our analysis including phase perturbations in the LO, we need to consider the perturbation voltage $V_{RF,n}$ found in Section C and its interaction with the full circuit including the source impedance Z_s. Therefore, we modify the block diagram in Figure 8 to that shown in Figure 10.

The I-to-V characteristic of the mixer generates the term $V_{RF,n}$ (Figure 9), which contains frequency components other than ω_s (specifically, $\omega_s \pm \omega_n$). Therefore, we cannot simply use LTI feedback equations to find V_{RF}, as $V_{RF,n}$ feeds back into the mixer, and can generate more terms at $\omega_s \pm \omega_n$. To solve this, we can use the fact that the voltages and currents at ω_s and $\omega_s \pm \omega_n$ can be treated separately and superposed. So we re-formulate Figure 10 into Figure 11. In Figure 11, there are two loops, one containing only components at ω_s, and the other containing components at $\omega_s \pm \omega_n$. This way, each loop can be solved using LTI analysis and the final voltage V_{RF} can still be found as the superposition of $V_{RF,s}$ and $V_{RF,n}$.

One final wrinkle is the fact that the $V_{RF,n}$ loop will generate its own new frequency terms (V_{RF,n^2}), shown in green in Figure 11. These terms will then need their own loop(s) to be analyzed properly, and this process could repeat infinitely. Luckily, the terms in $I_{RF,n}$ are of magnitude ϵ_n, so V_{RF,n^2} is of magnitude ϵ_n^2. As we have throughout this analysis, we will ignore terms with magnitude ϵ_n^2, and so the green blocks in Figure 11 can be ignored.

As in Section A, we would like to write a solely LTI model for the system to allow for LTI circuit analysis. This is not possible since V_{RF} contains components at frequencies other than the input frequency ω_s. However, if we define a fictitious perturbation input $V_{s,n} = A\sin[(\omega_s \pm \omega_n)t + \theta]$, we can define a transfer function from $V_{s,n}$ to $V_{RF,n}$. Because $V_{s,n}$ has the same magnitude and phase as V_s, equation (18) will accurately predict the $V_{RF,n}$ generated by the real input signal V_s.

$$V_{RF,n} = \left(\frac{\epsilon_n V_{s,n} Z_n(\omega_s \pm \omega_n)}{Z_{mix}(\omega_s) + Z_s}\right) - \left(\frac{V_{RF,n}}{Z_s}\right) Z_{mix}(\omega_s \pm \omega_n)$$

$$\frac{V_{RF,n}}{V_{s,n}} = \frac{\epsilon_n Z_n(\omega_s \pm \omega_n) Z_s}{(Z_{mix}(\omega_s) + Z_s)(Z_{mix}(\omega_s \pm \omega_n) + Z_s)} \quad (18)$$

E. Specifying $Z_{BB}(\omega)$ in Terms of ω_n

To predict the RF noise spectrum given a noisy LO, we must sweep ω_n from 0 to ∞ and superpose the results to see the magnitude of $V_{RF,n}$ for all the possible choices for ω_n. Then the RF spectrum can be plotted for a choice of ω_{LO}, ω_s, and Z_{BB}. As we did in our qualitative analysis, we will start by treating the LO phase perturbations as white (constant ϵ_n across ω_n), as would be generated by LO buffers, dividers, etc. Later we will use an oscillator phase noise model, where ϵ_n decreases at -20dB/decade as ω_n increases.

Since we are interested in the overall RF noise spectrum given white phase perturbations in the LO, we must include the effects of both the "$+\omega_n$" and "$-\omega_n$" components of equation (18). The "$+\omega_n$" term will produce voltage perturbations at the offset $+\omega_n$ from ω_s, while the "$-\omega_n$" term captures frequencies below ω_s. Therefore to derive the RF spectrum ($V_{spec,n}$) given white phase perturbations across all $\omega_n \in [0, \infty)$, we can use the following piecewise definition to properly superpose both components of $V_{RF,n}$:

$$\frac{V_{spec,n}(\omega)}{V_{s,n}} = \begin{cases} \dfrac{\epsilon_n Z_n(\omega_s - \omega_n) Z_s}{(Z_{mix}(\omega_s) + Z_s)(Z_{mix}(\omega_s - \omega_n) + Z_s)} & \omega < \omega_s \\ \dfrac{\epsilon_n Z_n(\omega_s + \omega_n) Z_s}{(Z_{mix}(\omega_s) + Z_s)(Z_{mix}(\omega_s + \omega_n) + Z_s)} & \omega \geq \omega_s \end{cases} \tag{19}$$

Next, we will re-write $V_{spec,n}$ solely in terms of absolute frequency ω. For $\omega < \omega_s$, $\omega = \omega_s - \omega_n$, and for $\omega \geq \omega_s$, $\omega = \omega_s + \omega_n$. With this substitution, both halves of the piecewise equation are identical, so we can simply write an equation with no restrictions on ω:

$$\frac{V_{spec,n}(\omega)}{V_{s,n}} = \frac{\epsilon_n Z_n(\omega) Z_s}{(Z_{mix}(\omega_s) + Z_s)(Z_{mix}(\omega) + Z_s)} \tag{20}$$

Now, we can define Z_{BB} to see what form $V_{spec,n}$ takes for specific baseband impedances. For simplicity, we will assume the baseband impedance is purely capacitive and the source impedance is purely resistive such that $Z_s = R_s = 50\Omega$. This models a bandpass N-path filter driven by a 50Ω source.

$$\begin{aligned} Z_{BB,i}(\omega) &= \frac{1}{j\omega C} \; \forall \; i \in [1, N] \\ Z_{BB}(\omega) &= Z_{BB,1} || Z_{BB,2} || \ldots || Z_{BB,N} \\ &= \frac{1}{j\omega NC} = \frac{1}{j\omega C_{tot}} \end{aligned} \tag{21}$$

We define Z_{BB} in terms of the total baseband capacitance C_{tot} because our model considers a quadrature baseband voltage rather than N separate, real baseband voltages. Because each of the N real voltages see a baseband capacitor of value C, the superposition of each of these voltages (V_{BB}) sees each of the baseband impedances ($Z_{BB,i} \; \forall \; i \in [1, N]$) in parallel. Therefore, we use the total baseband capacitance, C_{tot}. Substituting Z_{BB} into equation (20) and setting $Z_s = R_s$ gives:

$$\begin{aligned} \frac{V_{spec,n}}{V_{s,n}} &= \frac{2jC_{tot}R_s\epsilon_n\omega_{LO}\left(\omega^2 - \omega_s^2\right)}{K[2j\omega + C_{tot}R_s(\omega_{LO}^2 - \omega^2)]} \\ K &= 2j\omega_s + R_s C_{tot}(\omega_{LO}^2 - \omega_s^2) \end{aligned} \tag{22}$$

Examining equation (22), we see that there will always be a zero (and so suppression of noise) at the signal frequency ($\omega = \omega_s$ or $\omega_n = 0$). Additionally, we can see the magnitude of the denominator is minimized at $\omega = \omega_{LO}$, i.e. there is a noise peak around the LO frequency ω_{LO} (as long as $\omega_s \neq \omega_{LO}$, in which case the notch from the zero at ω_s will dominate). Additionally, if $\omega \to \infty$, this expression settles to one value, but if $\omega \to 0$, it settles to a different value. This means that as you move away from ω_s in either direction, after the possible peak at ω_{LO}, moving toward DC settles to a different value then moving toward higher frequencies. Plots of this function for a few choices of ω_s are shown in Figures 12 and 13. In both plots we see the zero at ω_s creates a notch, while the peak occurs at ω_{LO}. We can also see how the white noise level set far from ω_{LO} settles to different values as long as $\omega_s \neq \omega_{LO}$.

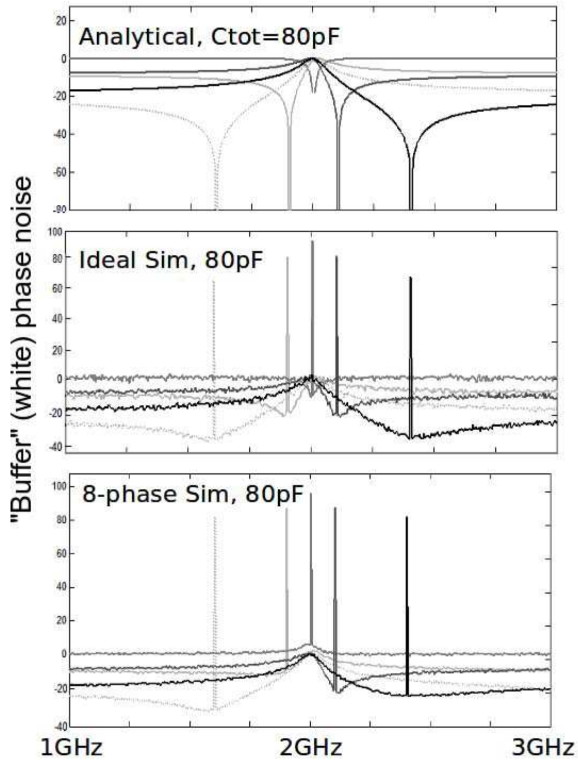

Fig. 12. MATLAB numerical simulation results with $F_{LO} = 2GHz$ for $C_{tot} = 80pF$ and several values of F_s given white phase noise. F_s is swept through the following values with darker lines indicating higher frequencies: $F_s = \{1.6$ GHz, 1.9 GHz, 2 GHz, 2.1 GHz, 2.4 GHz$\}$. All spectra are plotted in dB.

F. Modelling Non-White Phase Noise

To find the RF noise profile with any desired symmetrical power spectrum of phase noise, the steps of Section E can be repeated, but with a few small changes.

First, instead of being a constant, ϵ_n must be a function of ω_n. We choose ϵ_n to match the desired power spectrum—for example we will choose a -20dB/decade roll-off as ω_n increases to model oscillator-style phase noise. Choosing a desired baseband impedance Z_{BB}, allows one to write an expression for $\frac{V_{spec,n}}{V_{s,n}}$. It is worth noting that any power spectrum of phase noise can be modeled this way, assuming the largest value of ϵ_n across frequency does not violate the assumption $\epsilon_n << 1$.

To proceed with our example, we define ϵ_n as follows:

$$\epsilon_n = \frac{\epsilon_0}{|\omega_n|} = \frac{\epsilon_0}{|\omega - \omega_s|} \tag{23}$$

where ϵ_0 is a constant used to set the overall noise power, and ω_n is, as always, the frequency offset of the LO perturbation, implying a perturbation on the LO spectrum at $\epsilon_n = \frac{\epsilon_0}{|\omega_n|} = \frac{\epsilon_0}{|\omega - \omega_{LO}|}$. However, we are interested in the

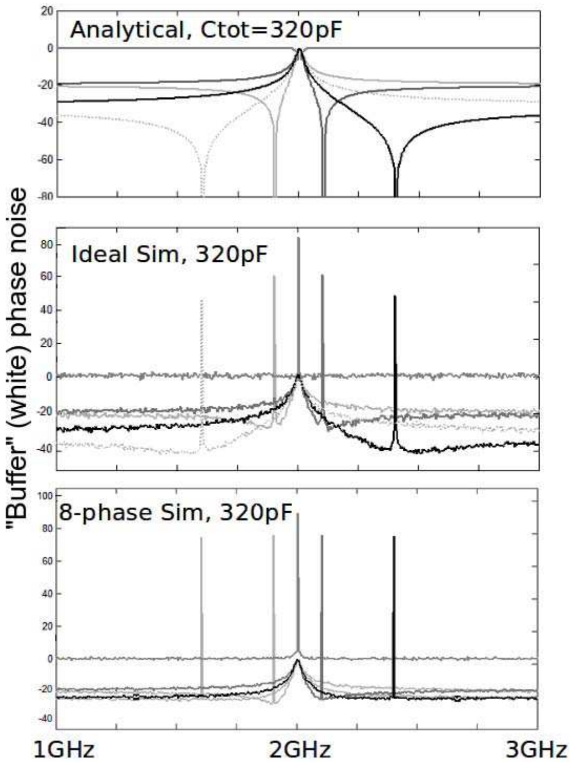

Fig. 13. MATLAB numerical simulation results with $F_{LO} = 2GHz$ for $C_{tot} = 320pF$ and several values of F_s given white phase noise. F_s is swept through the following values with darker lines indicating higher frequencies: $F_s = \{1.6\text{ GHz}, 1.9\text{ GHz}, 2\text{ GHz}, 2.1\text{ GHz}, 2.4\text{ GHz}\}$. All spectra are plotted in dB.

output RF spectrum, where ϵ_n is the coefficient of $V_{RF,n}$ which appears at $\omega_s \pm \omega_n$. Therefore, close-in phase noise (small ω_n) appears around ω_s at the RF port instead of ω_{LO}, as written in equation (23).

Additionally, note that for a real LO chain, noise at large offsets (large ω_n) is dominated by white noise rather than this -20dB/decade characteristic. Therefore, by choosing ϵ_n as ω_n we will only accurately predict the spectrum near ω_{LO}. If we proceed considering this limitation, equation (22) becomes:

$$\frac{V_{spec,n}}{V_{s,n}} = \frac{2jC_{tot}R_s\epsilon_0\omega_{LO}(\omega + \omega_s)}{K[2j\omega + C_{tot}R_s(\omega_{LO}^2 - \omega^2)]} \tag{24}$$

Notice that there is no longer a zero near $\omega = \omega_s$, as the phase noise peak around $\omega_n = 0$ perfectly cancels that zero. Otherwise, the equation is unchanged, implying the noise peak around ω_{LO} remains for all choices of ω_s. Plots of equation (24) for frequencies near ω_{LO} are shown in Figures 14 and 15. As expected, there is a noise peak at ω_{LO} for all values of ω_s, and there is no longer a notch around ω_s.

For greater than -20dB/decade of noise roll-off, such as the -30dB/decade that occurs close-in due to oscillator flicker noise, a noise peak will appear around ω_s, but reduced in slope to -10dB per decade of offset in ω_n.

IV. Simulation and Measurement Results

In order to confirm the above analysis, we performed numerical simulations in MATLAB and Cadence. We also confirmed our results with measurements of a frequency-scaled, board-level implementation of an N-path filter.

A. MATLAB Simulations

In MATLAB, we first implemented a numerical version of the mathematics described above, where the LO is described by quadrature sinusoids generated from a time-series of noisy phases, and the code computes explicit current-mode down-conversion, baseband integration, and voltage upconversion, all interacting with a 50-ohm RF signal source. We also developed a MATLAB model of an 8-phase passive mixer, with 8 switches whose conductance varies in time according to a similar time-series of noisy phase. In each case the RF sinusoidal input was introduced through a resistance R_s, and swept in frequency around a constant LO frequency ($F_{RF} = 1.6$GHz, 1.9GHz, 2 GHz, 2.1GHz and 2.4GHz, for $F_{LO} = 2$GHz). The resulting RF voltage time-series was then Fourier-transformed to compute a power spectrum in each case. Power spectra were averaged across many simulations. Comparisons of our analytical results, ideal mixer simulations and 8-phase switched simulations are shown in Figures 12 and 13 for white phase noise. The simulation results share many properties with our model, including a noise peak around the LO, and notching around the RF signal. However, we see that the depth of the notch around F_s is shallower for numerical simulations in general—especially for the 8-phase switch simulations. It appears that this is a consequence of harmonic interactions with the white phase noise folding back from higher harmonics and setting a noise floor. Since we neglect harmonic conversion effects in our model, any phase noise conversion due to those harmonics will not appear in the analytical plots. Nonetheless, the analytical predictions hold regarding the general shape of noise on the RF port due to phase noise.

Also of interest is the case where phase noise is non-white, but follows the -20dB/decade slope associated with oscillator phase noise. We simulated this by generating phase noise as a cumulative phenomenon over time (i.e. as a random walk) as is seen in real oscillators. Our analysis predicts that this noise peaking should be counter-acted by the notch (zero) associated with $\omega_n \to 0$. This should reduce the effects of noise folding in from harmonics, as noise is now concentrated around the LO. Indeed, we see (in Figures 14 and 15) that for such oscillator-like noise, analysis and numerical simulation are almost perfectly identical. Furthermore, as before the noise is clearly larger close to the LO frequency, and the noise increases overall as $|\omega_{LO} - \omega_s|$ decreases.

The actual shape of the noise is set by the filter properties of the mixer, and not that of the phase noise. This can be seen in Figure 16, where the spectrum of oscillator-like noise generated for our MATLAB simulations is compared with the output noise spectrum. The output follows the 1-pole lowpass characteristic of Z_{BB}, as evidenced by the discrepancy between the two curves close to F_{LO}, where the phase noise forms a sharp peak while the output noise flattens out due to the flat passband of $Z_{mix}||Z_s$ for very small ω_n (the single sharp peak at F_{LO} is associated with the signal tone at F_{LO}).

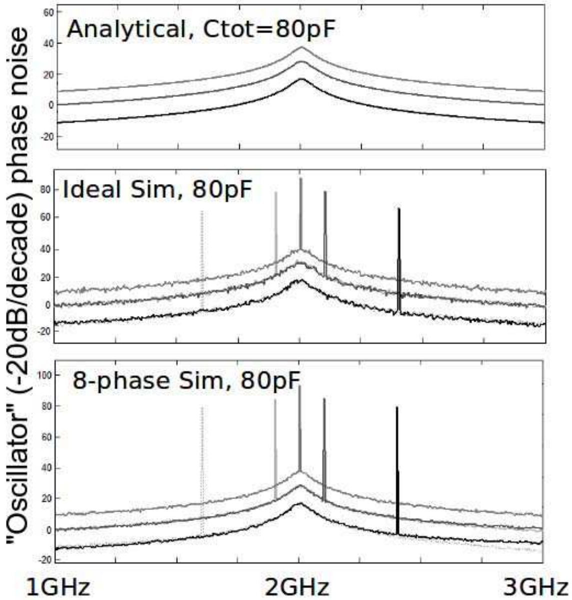

Fig. 14. MATLAB numerical simulation results with $F_{LO} = 2GHz$ for $C_{tot} = 80pF$ and several values of F_s given oscillator-style phase noise. F_s is swept through the following values with darker lines indicating higher frequencies: $F_s = \{1.6$ GHz, 1.9 GHz, 2 GHz, 2.1 GHz, 2.4 GHz$\}$. All spectra are plotted in dB.

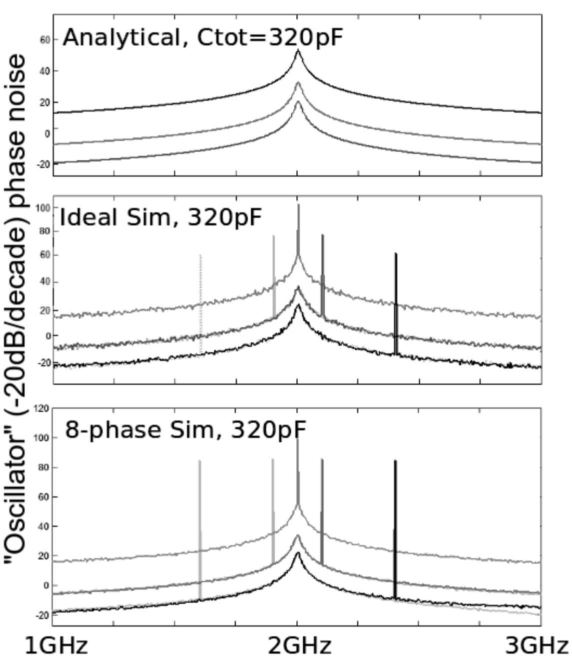

Fig. 15. MATLAB numerical simulation results with $F_{LO} = 2GHz$ for $C_{tot} = 80pF$ and several values of F_s given oscillator-style phase noise. F_s is swept through the following values with darker lines indicating higher frequencies: $F_s = \{1.6$ GHz, 1.9 GHz, 2 GHz, 2.1 GHz, 2.4 GHz$\}$. All spectra are plotted in dB.

B. Cadence Simulations

We also confirmed our analysis in Cadence by simulating real passive mixer and LO generation circuits similar to those reported in [7]. These simulations were performed by adding a phase perturbation at some offset ω_n from a sinusoidal

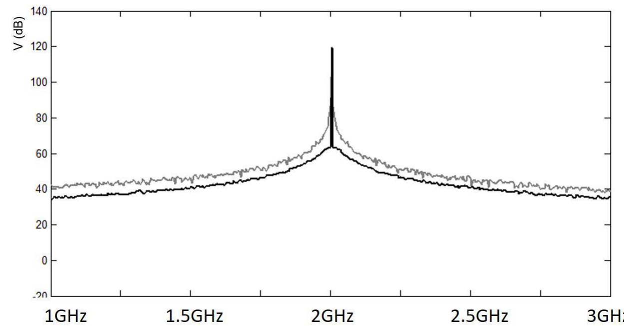

Fig. 16. Comparison of the oscillator-like phase noise used in our numerical simulation (lighter curve) and the output spectrum for $F_s = F_{LO}$ (darker curve). The output noise spectrum's shape is determined by the baseband impedance, not the oscillator's phase noise skirt.

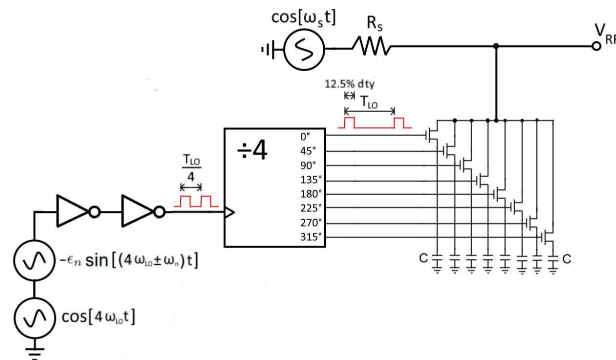

Fig. 17. A diagram of the Cadence simulation used to generate Figure 18. The LO pulses are generated using a frequency divider, and the phase perturbations are injected at the initial LO input at $4\omega_{LO}$. These LO pulses go into an 8-phase passive mixer loaded with capacitors on the baseband port. Finally, the signal source drives V_{RF} through $R_s = 50\Omega$.

source at $4 * F_{LO}$, passing that into real LO generation circuits which divide the frequency by 4 and produce 8-phase non-overlapping pulses for the mixer switches, and then injecting a signal at ω_s into the RF port of a passive mixer (this LO generation method is discussed in more detail in [7]). A schematic of this setup is given in Figure 17. By sweeping ω_n over a wide frequency range and superposing the results, we can build a transfer function approximately equivalent to the RF power spectrum, as long as ϵ_n is kept small. The results of schematic simulations are shown in Figure 18 for $C_{tot} = 320$pF, indicating a transfer function from phase perturbations to voltage perturbations in V_{RF} with a similar frequency response to those seen in our analysis.

Note that this simulation is more akin to the impact of a spur in the LO (as opposed to broad-band noise). As such, it captures the same kind of transfer function as the analysis in Section III, but does not replicate the harmonic effects seen with wide-band white noise in Figures 12 and 13.

C. Frequency-Scaled Implementation Measurements

Finally, we constructed a PCB according to the circuit in Figure 19 to demonstrate our model using real circuits. The board allowed us to repeat the method used in the Cadence simulation (sweeping an explicit phase perturbation at the

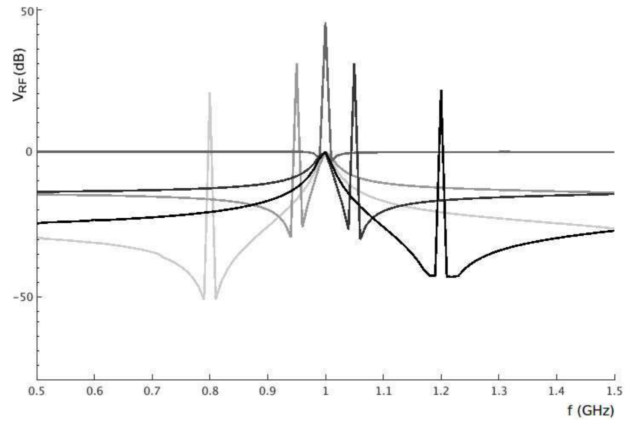

Fig. 18. Simulations of the Cadence circuit with different values of ω_n superposed to generate a full RF spectrum. $F_{LO} = 1$ GHz, C = 40pF ($C_{tot} = 320$pF), and F_s is swept from 800 MHz to 1200MHz. Darker curves correspond to higher source frequencies (F_s). White phase noise was used as in Figures 12 and 13, however the fractional bandwidth here is different, as in our MATLAB simulations $F_{LO} = 2$ GHz.

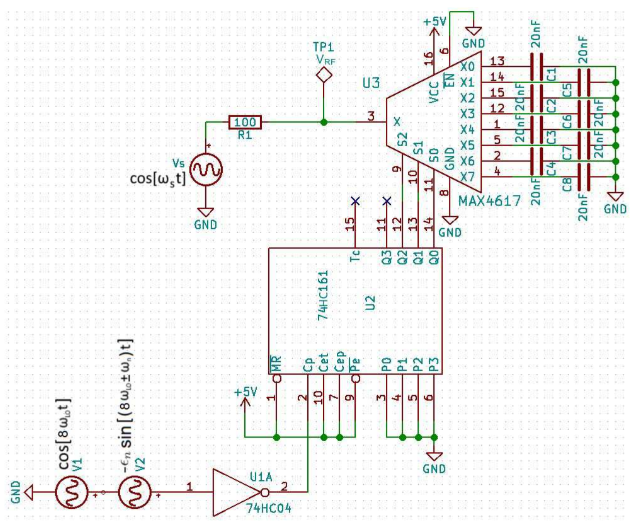

Fig. 19. The schematic for our board-level N-path filter implementation. LO pulses are generated internally by the MAX4617 based on the BB port selected by the free-running 74HC161 counter. Unlike in the Cadence circuit, this method requires the LO to operate at eight times the desired center frequency. A 100Ω source impedance was chosen instead of 50Ω to keep the effects of switch resistance negligible (the MAX4617 features $R_{ON} = 10\Omega$).

offset ω_n) with real hardware, albeit at lower frequency. Figure 20 shows the results of sweeping ω_n for multiple source frequencies. The real-world results match almost perfectly with our model and with the Cadence simulation. The only deviation from our model is a small amount of power at $2F_{LO} - F_s$, which is due to imperfect image cancellation caused by the fact that the MAX4617 has some LO pulse overlap when switching between baseband ports.

It is worth noting that one limitation of our model is the assumption that mixing can be modeled with simple multiplication. One way this is evident is in the discrepancy in the depth of notches in our numerical simulations. Another is the fact that in any simulation where the 8-phase switching aspect of the mixers are captured, we see additional noise peaks around LO harmonics ($2F_{LO}, 3F_{LO}, \ldots$). Because we do not account for harmonic mixing in our analysis, our predicted

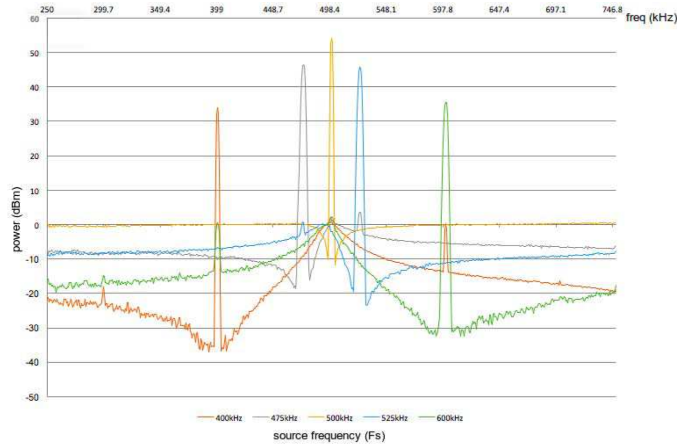

Fig. 20. The output spectrum of V_{RF} from Figure 19. Results are shown using the following values: $F_{LO} = 500$kHz, $R_s = 100\Omega$, and $C_{tot} = 160$nF.

spectra are only accurate for $F \in [\frac{F_{LO}}{2}, \frac{3F_{LO}}{2}]$, as closer to $2F_{LO}$ the 2nd harmonic mixing effects become dominant.

V. CONCLUSION

In this paper, we developed a framework for analyzing phase noise in passive mixer circuits, and we specifically investigated the behavior of N-path filters given a noisy LO. Our analysis assumed no harmonic mixing, and only small phase perturbations in the LO, and is therefore only accurate for frequencies near F_{LO}. For a white phase noise input, we see a peak in the noise floor at F_{LO}, and a notch at the input frequency F_s. If oscillator-like phase noise with a -20dB/decade roll-off is assumed, the notch perfectly cancels the expected peak around F_s, leaving only the peak at F_{LO}. Additionally, the shape of the peak around F_{LO} is not determined by the power spectrum of the LO phase noise, but rather by the baseband impedance of the N-path filter. The height of the noise peak around F_{LO} is also dependent on the strength of the signal tone after the effects of the N-path filter. In other words, the RF noise floor due to LO phase noise is not constant as F_s changes—rather it decreases as F_s diverges from F_{LO}.

The implication for RF design using N-path filters is that, while the noise behavior differs in some ways from conventional wisdom, low phase noise is still a critical specification for the LO if low noise is crucial in the signal path of the system when strong RF signals are present. Although the noise contributed by out-of-band signals diminishes as F_s diverges from F_{LO}, any in-band signal will interact strongly with the LO to produce the dominant noise voltage (except very close to F_s). Therefore, as long as there is any in-band signal to pass, an N-path filter will reduce the system's SNR, unless the LO itself has negligible phase noise. If the only frequencies of interest are those very close to F_{LO}, LO phase noise contributes little given an in-band tone, but out-of-band inputs will still produce a noise peak near F_{LO}, degrading the noise performance very close to F_{LO}.

In summary, we show that, unsurprisingly, phase noise and/or spurs in the LO of a shunting passive N-path mixer generates voltage noise and/or spurs in the presence of strong RF signals. As with standard up- and downconversion mixers, the magnitude of the noise depends on the magnitude of the phase noise, the magnitude of the RF signal, and their frequency separation. However, this noise spectrum that appears on the RF port is somewhat more complex than what is encountered in simple up- or downconversion. Noise and spurs appearing on the RF port are generally largest close to the LO frequency, regardless of the precise frequency of an out-of-band RF signal. Conversely, as the RF signal's frequency approaches the LO frequency, out-of-band noise and spurs will increase in amplitude. Finally, under all conditions, noise and spurs that appear close to the RF signal frequency are suppressed. Thus, when designing N-path filters to selectively suppress or pass strong RF signals, these results can provide useful guidance in the design and specification of LO circuits, regarding phase noise and acceptable spurs. In addition, the analytical framework presented here can likely be generalized for a variety of other related circuits, such as N-path notch filters [4]–[6], tunable degeneration [7], and LTV circulators [8].

Appendix

To expand and simplify, V_{RF}, we first substitute the expressions for $V_{BB,I}$ and $V_{BB,Q}$ from equation (14) into equation (15) to get equation (25) shown at the bottom of the page. Equation (25) can then be re-written as the sum of 1) the previously found signal term $V_{RF,s}$, 2) a term with magnitude ϵ_n, and 3) a term with magnitude ϵ_n^2, however we will ignore the ϵ_n^2 term as we have assumed $\epsilon_n << 1$.

To arrive at equation (26), shown at the bottom of the page, we re-arrange equation (25) such that $V_{RF,s}$ holds all the signal terms found in Section A, and we will write out the full ϵ_n term using baseband currents and Z_{BB} evaluated at each current's relevant frequency. Now, we would like to make equation (26) more manageable. Specifically, we would like V_{RF} in terms of $I_{RF,s}$, since the goal is to find the I-to-V characteristic of the passive mixer. To do this, we will break out various terms from equation (26) individually, and find that when we substitute in our original definitions for $I_{RF,s}$, $S_{LO,I}$, and $S_{LO,Q}$, they each simplify to $\pm\frac{\epsilon_n A}{2}\sin[(\omega_s \pm \omega_n)t \pm \phi_n]$, which will allow us to re-write equation (26) in a much simpler form.

A. Simplify "Low" Noise Term

First, we convert the "low" baseband term (N_{low}) into the time domain by plugging in our definitions for $S_{LO,s}$, as well as expressions for $I_{BB,In,low}$ and $I_{BB,Qn,low}$ found using our

$$\begin{aligned} V_{RF} &= V_{BB,I} * (S_{LO,Is} + \epsilon_n S_{LO,In}) + V_{BB,Q} * (S_{LO,Qs} + \epsilon_n S_{LO,Qn}) \\ &= \Big(\big[V_{BB,Is,low} + V_{BB,Is,high} + V_{BB,In,low} + V_{BB,In,high}\big] * [S_{LO,Is} + \epsilon_n S_{LO,In}]\Big) \\ &\quad + \Big(\big[V_{BB,Qs,low} + V_{BB,Qs,high} + V_{BB,Qn,low} + V_{BB,Qn,high}\big] * [S_{LO,Qs} + \epsilon_n S_{LO,Qn}]\Big) \end{aligned} \tag{25}$$

$$\begin{aligned} V_{RF} &= V_{RF,s} + \epsilon_n\Big[Z_{BB}(\omega_s - \omega_{LO} \pm \omega_n)(I_{BB,In,low} * S_{LO,Is} + I_{BB,Qn,low} * S_{LO,Qs}) \\ &\quad + Z_{BB}(\omega_s + \omega_{LO} \pm \omega_n)(I_{BB,In,high} * S_{LO,Is} + I_{BB,Qn,high} * S_{LO,Qs}) \\ &\quad + Z_{BB}(\omega_s + \omega_{LO})(I_{BB,Is,high} * S_{LO,In} + I_{BB,Qs,high} * S_{LO,Qn}) \\ &\quad + Z_{BB}(\omega_s - \omega_{LO})(I_{BB,Is,low} * S_{LO,In} + I_{BB,Qs,low} * S_{LO,Qn})\Big] \end{aligned} \tag{26}$$

$$\begin{aligned} N_{low} &= I_{BB,In,low}(\omega) * S_{LO,Is}(\omega) + I_{BB,Qn,low}(\omega) * S_{LO,Qs}(\omega) \\ &\rightarrow I_{BB,In,low}(t) \cdot S_{LO,Is}(t) + I_{BB,Qn,low}(t) \cdot S_{LO,Qs}(t) \\ &= A\left(\frac{\epsilon_n}{2}\sin[(\omega_s - \omega_{LO} \pm \omega_n)t \pm \phi_n]\right) S_{LO,Is} + A\left(\frac{\epsilon_n}{2}\cos[(\omega_s - \omega_{LO} \pm \omega_n)t \pm \phi_n]\right) S_{LO,Qs} \\ &= \frac{\epsilon_n A}{2}\sin[(\omega_s \pm \omega_n)t \pm \phi_n] \end{aligned} \tag{27}$$

$$\begin{aligned} N_{high} &= I_{BB,In,high}(\omega) * S_{LO,Is}(\omega) + I_{BB,Qn,high}(\omega) * S_{LO,Qs}(\omega) \\ &\rightarrow I_{BB,In,high}(t) \cdot S_{LO,Is}(t) + I_{BB,Qn,high}(t) \cdot S_{LO,Qs}(t) \\ &= A\left(\frac{-\epsilon_n}{2}\sin[(\omega_s + \omega_{LO} \pm \omega_n)t \pm \phi_n]\right) S_{LO,Is} + A\left(\frac{\epsilon_n}{2}\cos[(\omega_s + \omega_{LO} \pm \omega_n)t \pm \phi_n]\right) S_{LO,Qs} \\ &= -\frac{\epsilon_n A}{2}\sin[(\omega_s \pm \omega_n)t \pm \phi_n] \end{aligned} \tag{28}$$

$$\begin{aligned} &\epsilon_n I_{RF,s}(\omega) * \big[S_{LO,Is}(\omega) * S_{LO,In}(\omega) + S_{LO,Qs}(\omega) * S_{LO,Qn}(\omega)\big] \\ &\rightarrow \epsilon_n I_{RF,s}(t)\big[S_{LO,Is}(t) \cdot S_{LO,In}(t) + S_{LO,Qs}(t) \cdot S_{LO,Qn}(t)\big] \\ &= \epsilon_n A\cos(\omega_s t) \cdot \Big[\cos(\omega_{LO}t)\sin[(\omega_{LO} \pm \omega_n)t \pm \phi_n] + \sin(\omega_{LO}t)\cos[(\omega_{LO} \pm \omega_n)t \pm \phi_n]\Big] \\ &= \epsilon_n A\cos(\omega_s t) \cdot \Big[\frac{-1}{2}\sin(\pm\omega_n t \pm \phi_n) + \frac{1}{2}\sin[(2\omega_{LO} \pm \omega_n)t \pm \phi_n] \\ &\qquad - \frac{1}{2}\sin(\pm\omega_n t \pm \phi_n) - \frac{1}{2}\sin[(2\omega_{LO} \pm \omega_n)t \pm \phi_n]\Big] \\ &= -\frac{\epsilon_n A}{2}\sin[(\omega_s \pm \omega_n)t \pm \phi_n] \end{aligned} \tag{29}$$

definition for $I_{RF,s}$ and equation 12 into equation (27), shown at the bottom of the previous page. After simplification, we find that the "low" baseband term only produces a single tone at $\omega_s \pm \omega_n$ in V_{RF}.

B. Simplify "High" Noise Term

We repeat the same work for N_{high}, as we did for N_{low}—again plugging in expressions for $I_{BB,In,high}$ and $I_{BB,Qn,high}$ derived from equation (12) into (28). Again, we get a single tone at $\omega_s \pm \omega_n$, although the sign is reversed compared with N_{low}.

C. Equivalent Expression in Terms of $I_{RF,s}$

Because both the "high" and "low" baseband components simplify to $\pm \sin[(\omega_s \pm \omega_n)t \pm \phi_n]$, we can replace them with another expression which simplifies to the same sine function, but which is written in terms of $I_{RF,s}$, $S_{LO,I}$, and $S_{LO,Q}$ rather than baseband currents. This will allow us to more clearly see how $I_{RF,s}$ generates V_{RF}.

We find that $\pm\epsilon_n I_{RF,s}[S_{LO,Is}(\omega) * S_{LO,In}(\omega) + S_{LO,Qs}(\omega) * S_{LO,Qn}(\omega)]$ can be substituted for N_{high} and N_{low} as long as the sign in front is correct, according to equation (29), shown at the bottom of the previous page.

It can be shown via the same process that the noise terms resulting from noisy upconversion of baseband signals also end up solely at $\omega_s \pm \omega_n$, and therefore the baseband currents in those terms there can also be replaced the expression in equation (29). Given all of these substitutions, equation (15) can be simplified to equation (16) as asserted in the text.

ACKNOWLEDGMENT

The authors would like to thank Mark Rich, Michael Mack, MeeLan Lee, and Daniel Yetso from Google, Inc. for their support and insight. This paper is dedicated to the memory of Mark Rich, who was an early supporter of our ideas, and without whom this work may not have existed.

REFERENCES

[1] L. E. Franks and I. W. Sandberg, "An alternative approach to the realization of network transfer functions: The N-path filter," *Bell Syst. Tech. J.*, vol. 39, no. 5, pp. 1321–1350, Sep. 1960.

[2] Y.-C. Hsiao, C. Meng, J.-S. Syu, C.-Y. Lin, S.-C. Wong, and G.-W. Huang, "5–6 GHz 9.4 mW CMOS direct-conversion passive-mixer receiver with low-flicker-noise corner," in *Proc. 7th Eur. Microw. Integr. Circuits Conf.*, Amsterdam, The Netherlands, Oct. 2012, pp. 301–304.

[3] A. Ghaffari, E. A. M. Klumperink, M. C. M. Soer, and B. Nauta, "Tunable high-Q N-path band-pass filters: Modeling and verification," *IEEE J. Solid-State Circuits*, vol. 46, no. 5, pp. 998–1010, May 2011.

[4] B. W. Cook, A. Berny, A. Molnar, S. Lanzisera, and K. S. J. Pister, "Low-power 2.4-GHz transceiver with passive RX front-end and 400-mV supply," *IEEE J. Solid-State Circuits*, vol. 41, no. 12, pp. 2757–2766, Dec. 2006.

[5] D. Murphy *et al.*, "A blocker-tolerant, noise-cancelling receiver suitable for wideband wireless applications," *IEEE J. Solid-State Circuits*, vol. 47, no. 12, pp. 2943–2963, Dec. 2012.

[6] D. Yang, C. Andrews, and A. Molnar, "Optimized design of N-phase passive mixer-first receivers in wideband operation," *IEEE Trans. Circuits Syst. I, Reg. Papers*, vol. 62, no. 11, pp. 2759–2770, Nov. 2015.

[7] H. Yüksel *et al.*, "A wideband fully integrated software-defined transceiver for FDD and TDD operation," *IEEE J. Solid-State Circuits*, vol. 52, no. 5, pp. 1274–1285, May 2017.

[8] N. Reiskarimian, J. Zhou, and H. Krishnaswamy, "A CMOS passive LPTV nonmagnetic circulator and its application in a full-duplex receiver," *IEEE J. Solid-State Circuits*, vol. 52, no. 5, pp. 1358–1372, May 2017.

[9] F. Behbahani, Y. Kishigami, J. Leete, and A. A. Abidi, "CMOS mixers and polyphase filters for large image rejection," *IEEE J. Solid-State Circuits*, vol. 36, no. 6, pp. 873–887, Jun. 2001.

[10] S. Yazdi and M. Green, "A precise 360°-range phase detector based on an N-path filter," in *Proc. 14th IEEE Int. New Circuits Syst. Conf. (NEWCAS)*, Vancouver, BC, Canada, Jun. 2016, pp. 1–4.

[11] S. Hameed, M. Rachid, B. Daneshrad, and S. Pamarti, "Frequency-domain analysis of *N*-path filters using conversion matrices," *IEEE Trans. Circuits Syst. II, Exp. Briefs*, vol. 63, no. 1, pp. 74–78, Jan. 2016.

[12] C. Andrews and A. C. Molnar, "Implications of passive mixer transparency for impedance matching and noise figure in passive mixer-first receivers," *IEEE Trans. Circuits Syst. I, Reg. Papers*, vol. 57, no. 12, pp. 3092–3103, Dec. 2010.

[13] H. Khatri, P. S. Gudem, and L. E. Larson, "Distortion in current commutating passive CMOS downconversion mixers," *IEEE Trans. Microw. Theory Techn.*, vol. 57, no. 11, pp. 2671–2681, Nov. 2009.

[14] E. S. Atalla, F. Zhang, P. T. Balsara, A. Bellaouar, S. Ba, and K. Kiasaleh, "Time-domain analysis of passive mixer impedance: A switched-capacitor approach," *IEEE Trans. Circuits Syst. I, Reg. Papers*, vol. 64, no. 2, pp. 347–359, Feb. 2017.

[15] F. Qazi and J. Dąbrowski, "Clock phase imbalance and phase noise in RF N-path filters," in *Proc. Eur. Conf. Circuit Theory Design (ECCTD)*, Trondheim, Norway, Aug. 2015, pp. 1–4.

Thomas Tapen received the B.S. degree in electrical engineering from Cornell University, Ithaca, NY, USA, in 2015.

His current research interests include mixed-signal integrated circuit design.

Zachariah Boynton received the B.S. degree in electrical engineering from the University of Massachusetts Amherst, Amherst, MA, USA, in 2015.

His current research interests include RF, analog, and mixed-signal circuit design.

Hazal Yüksel (S'14) received the B.S. degree in electrical engineering with a minor in mathematics from Duke University, Durham, NC, USA, in 2012. She is currently pursuing the Ph.D. degree in electrical engineering with Cornell University, Ithaca, NY, USA.

Her current research interests include signal processing and adaptive radios.

Alyssa Apsel (M'03–SM'10) received the B.S. degree from Swarthmore College, Swarthmore, PA, USA, in 1995, and the Ph.D. degree from Johns Hopkins University, Baltimore, MD, USA, in 2002. She joined Cornell University, Ithaca, NY, USA, in 2002, where she is currently a Professor of electrical and computer engineering. She has authored or co-authored over 100 referenced publications in related fields of RF mixed-signal circuit design, ultralow-power radio, interconnect design and planning, photonic integration, and process invariant circuit design techniques, resulting in eight patents and several pending patent applications. Her current research interests include power-aware mixed-signal circuits and design for highly scaled CMOS and modern electronic systems.

Dr. Apsel received best paper awards at ASYNC in 2006 and the IEEE SiRF in 2012, the College Teaching Award in 2007, and the National Science Foundation CAREER Award in 2004. She was selected by *Technology Review Magazine* as one of the Top Young Innovators in 2004. She had a MICRO Top Picks Paper in 2006. She has served as an Associate Editor of various journals, including the IEEE TRANSACTIONS ON CIRCUITS AND SYSTEMS I and II, and has also served as the Chair of the Analog and Signal Processing Technical Committee of ISCAS 2011, as the Deputy Editor-in-Chief of the *IEEE Circuits and Systems (CAS) Magazine*, and on the Board of Governors of the IEEE CAS Society.

Alyosha Molnar received the B.S. degree from the Swarthmore College in 1997. He was with Conexant Systems as an RFIC Design Engineer, from 1998–2001, where he jointly developed their first-generation direct-conversion receiver for the GSM cellular standard. Starting graduate school at University of California at Berkeley in 2001, he was involved in early, ultralow-power radio transceivers for wireless sensor networks, and then joined a retinal neurophysiology group, where he was also involved in dissecting the structure and function of neural circuits in the mammalian retina. He joined the Faculty at Cornell University in 2007, where he is an Associate Professor and focused on software-defined radios, neural interface circuits, integrated imaging techniques, and ultralow-power sensing.